International Journal of Thin Films Science and Technology

http://dx.doi.org/10.18576/ijtfst/150106

Modeling Pressure and Distance Effects on Particle Transport in PVD Sputtering Using a 3D Monte Carlo Approach

Abdelkader Bouazza [1] *and Mark-Edgard Tchanolo*[2,*]

[1] L2GEGI Laboratory, University of Tiaret, 14000 Tiaret, Algeria
[2] University of Science and Technology of Benin, Cotonou, 2332, Benin

Received: 11 Sep. 2025, Revised: 27 Nov. 2025, Accepted: 27 Dec. 2025
Published online: 1 Jan. 2026

Abstract: Thin-film technologies continue to advance in response to industrial requirements for improved performance, precision, and reliability. Among deposition techniques, physical vapor deposition (PVD) via sputtering is widely recognized for its capacity to generate high-quality films with controlled morphology and reproducible characteristics. This study employs a three-dimensional Monte Carlo simulation model to investigate the transport behavior, energy evolution, and angular distribution of sputtered particles during thin-film formation, accounting for elastic collisions with background argon gas. The influence of chamber pressure and target–substrate spacing is evaluated in detail. Results show that increasing pressure or distance produces more uniform particle distributions, consequently improving film homogeneity. Although the present work is purely computational, the obtained trends are consistent with previously reported Monte Carlo simulations and experimentally supported transport studies.

Keywords: engineering thin-film materials; plasma particle transport; Monte Carlo simulation.

1. Introduction

Thin films have become essential components in a wide spectrum of modern technologies, ranging from microelectronics and optical devices to solar energy systems, biomedical tools, and magnetic materials. Their growing importance stems from the ability to tailor their electrical, mechanical, and structural properties to meet the increasingly demanding requirements of advanced applications. Sputtering is a widely used physical vapor deposition (PVD) technique for producing thin films with controlled morphology, high purity, and reproducible characteristics. It enables excellent uniformity over extended surfaces, precise control of thickness, strong adhesion, and compatibility with a wide variety of materials, making it a preferred choice in industrial and research environments. [1-5].

To further optimize deposition quality, simulation tools have become indispensable for understanding the interaction between sputtered atoms and the background gas during transport. The Monte Carlo (MC) approach, in particular, has proven to be a powerful statistical tool for studying how sputtered particles lose energy, change direction, and undergo collisions before reaching the substrate. Since the microstructure of the deposited film is strongly influenced by these parameters, modeling their evolution provides valuable insight into the mechanisms governing film growth and helps refine sputtering conditions for improved performance [6-11].

Although previous studies have examined several aspects of sputtering, the combined effects of particle energy, angular distribution, and environmental parameters such as chamber pressure and target–substrate distance remain central to predicting thin-film characteristics. These factors play a decisive role in determining film uniformity, crystallographic texture, and surface quality. Understanding their influence is therefore essential for designing efficient sputtering systems and for meeting the stringent requirements of modern materials engineering applications. [12-17].

The objective of this work is to develop a three-dimensional Monte Carlo simulation model to analyze the transport of sputtered metal (Cu, Al, Ag) and semiconductor (Ge, Si, Te) atoms under identical sputtering conditions. The influence of chamber pressure and target–substrate distance on particle energy distributions and arrival flux is systematically investigated in order to provide quantitative guidelines for process optimization.

2. Monte Carlo Simulation and Modeling

The transport of sputtered atoms from the target to the substrate involves a complex sequence of collisions, energy losses, and directional changes that significantly influence the final thin-film structure. To analyze these mechanisms, a three-dimensional Monte-Carlo (MC) model was developed to simulate the trajectory, scattering behavior, and energy evolution of individual atoms ejected during the sputtering process. Each particle emitted from the target is assigned an initial energy and direction based on the Sigmund–Thompson distribution, which provides a realistic description of sputtering emission conditions. These initial

*Corresponding author E-mail: phdny25@yahoo.com

parameters serve as the starting point for tracking particle motion throughout the chamber.

Throughout transportation modeling, Cu particle collisions with unique background Ar gas particles are simulated at periods defined by mean free path estimations, with each collision event regarded as an elastic, momentum-transferring event that modifies the Cu atom's velocity vector. The program tracks the materials particles in the region between the sputtering target and the substrate, one at a time. At the close of the process, we have several particles per unit of surface on every location, allowing us to determine the thickness throughout the chamber.

To modulate the entire particle trajectory, we require the emission circumstances (approximate location of the emission site, sputtering direction, starting energy, Etc.) and the transmission throughout the chamber (series of free paths and interactions that affect the distribution in direction and energy). The ejected atoms are supposed to solely collide with argon molecules (and not with other ejected atoms).

This hypothesis is supported by the fact that the concentration of ejected atoms is minimal compared to that of the background gas in the circumstances utilized. In addition, the gas density in the targets-to-substrate gap is uniform. The Sigmund–Thompson distribution governed the energy of ejected particles and their angular distribution from the targets [18- 20].

$$f(E,\beta) = \frac{2U_{sb}E}{(E+U_{sb})^3}\frac{\cos(\beta)}{\pi} \tag{1}$$

Usb is the target material's surface binding energy, often considered the sublimation energy, and β is the velocity vector's angle concerning the axial direction [21], the following equation is used to compute the specific angle and energy of a primary ejected particle at the target using two random numbers ($NR1$,

$NR2$) distributed equitably between 0 and 1.

$$\begin{aligned} N_{R1}(\beta) &= \int_0^{\infty}\int_0^{\beta} 2\pi\sin(\beta)\cdot\frac{2U_{sb}E}{(E+U_{sb})^3}\frac{\cos(\beta)}{\pi}\,\mathrm{d}E\,\mathrm{d}\beta \\ N_{R2}(E) &= \int_0^{E}\int_0^{\frac{\pi}{2}} 2\pi\sin(\beta)\cdot\frac{2U_{sb}E}{(E+U_{sb})^3}\frac{\cos(\beta)}{\pi}\,\mathrm{d}E\,\mathrm{d}\beta \end{aligned} \tag{2}$$

that leads to

$$\begin{aligned} &\beta = \left(\frac{1}{2}\right)\arccos(1-2N_{R1}) \\ &E^2(N_{R2}-1) + E(2U_{sb}R_2) + U_{sb}^2N_{R2} = 0 \end{aligned} \tag{3}$$

The positive roots generate E. And the azimuthal ejection angle ϕ (angle of the velocity vector's projection in the x, y plane, concerning the x-axis) is produced uniformly between 0 and 2π by a random number $NR3$ in 0 and 1 range,

$$\phi = 2\pi N_{R3} \tag{4}$$

No association has been observed between the ejection angle and energy. The x and y coordinates of the initial stage are also determined based on randomly selected value $NR4$ such that:

$$\begin{aligned} x &= \mathrm{r}N_{R4}\sin(\phi) \\ y &= \mathrm{r}N_{R4}\cos(\phi) \end{aligned} \tag{5}$$

The z-coordinates start at zero. The target radius r was set to 4 cm in our calculations. Distribution homogeneity may enhance as the number of particles increases, precisely what happens during sputtering.

The gas-phase travel mechanisms of an ejected atom were determined using the MC method. We simulated the trajectory of each atom by computing the free path between the ejection and the first collision position and then between two subsequent collisions, using the collision factors (impact factor, sputtering atom deviation, and energy loss). In contrast to the important kinetic energy of sputtered species, the mobility of background gas atoms is ignored. As a result, the sputtered atom's mean free path λp is obtained by

$$\lambda_{\mathrm{p}} = \frac{k_BT}{\left(r_{\mathrm{gas}}+r_{\mathrm{atom}}\right)^2\pi P} \tag{6}$$

kB is the constant of Boltzmann, T and P are the plasma gas temperature, and pressure, respectively, and $rgas$ and $ratom$ are the atomic radii of the working gas and ejected atom.

The distance λ traveled by a particle between two subsequent interactions corresponds with the mean free path λp via the Monte Carlo method.

$$\lambda = -\lambda_p\ln(N_{R5}) \tag{7}$$

$NR5$ is a random value in the 0 and 1 range, and the material atom collides with a background gas particle after each λ; the scattering process was described using a hard-sphere collision technique with an energy- dependent value for $rgas$ and $ratom$ [22].

Also, a Born–Mayer type interatomic potential was employed to estimate the interatomic separation of the sputtered atom and background gas atom rgp = ($rgas$ + $ratom$) (atomic radii summation). The repulsive component of the particle-particle potential was estimated by Abrahamson [23], and the potentials were expressed in the range 0.8 Å < rgp < 1.9 Å. Within these conditions, the Born–Mayer form of scattering potential occurs.

$$V(r) \approx \left(A_{\mathrm{sp}}A_{\mathrm{gas}}\right)^{0.5}\exp\left|-\left(\frac{b_{sp}+b_{gas}}{2}\right)r\right| \tag{8}$$

Asp, $b$sp, Agas, and $b$gas are the Born-Mayer constants for sputtered and background gas particles. The mean free path has been calculated using the minimum interatomic separation rgp of the sputtered atom and the colliding gas atom for a center collision with the Esp kinetic energy of the sputtered atom, disregarding the thermal motion of the

background gas atoms. The mean free path diminishes causing the ejected particle to collide with gas molecules. Each impact causes the ejected particle's direction to shift and energy lost.

$$r_{gp} = \left(r_{gas} + r_{atom}\right) \approx -\frac{2}{b_{\mathrm{sp}}+b_{\mathrm{gas}}} \ln \frac{E_{sp}}{(A_{sp}A_{gas})^{\frac{1}{2}}} \quad (9)$$

The scattering angle χ concerning the laboratory frame of reference and the energy loss rate Ek are supplied by the hard-sphere collision model used to examine the track of the sputtered atom.

$$\tan\chi = \frac{\sin(\pi-2\theta)}{\frac{m_1}{m_2}+\cos(\pi-2\theta)} \quad (10)$$

$$E_{\mathrm{k}} = \frac{(m_1-m_2)^2\cos^2\theta+(m_1+m_2)^2\sin^2\theta}{(m_1+m_2)^2} \quad (11)$$

where m_1 and m_2 are the masses of sputtered and the plasma gas atoms, respectively, and θ formed by a line passing between the centers of sputtered atoms and the background atom before the collision.

$$\theta = \arcsin(N_{R6})^{\frac{1}{2}} \quad (12)$$

where $NR6$ is a random number in [0,1], the azimuthal angle of scattering ψ is determined by a random number $NR6$:

$$\psi = 2\pi N_{R6} \quad (13)$$

The new direction in three-dimensional space, the new angles θ and ϕ are calculated from the angles θ_0 and ϕ_0 before scattering and from the scattering angle χ and the azimuthal angle of scattering ψ, by the transformation of the coordinate frame of reference:

$$\begin{pmatrix}\sin(\theta)\cos(\phi)\\ \sin(\theta)\sin(\phi)\\ \cos(\theta)\end{pmatrix} =$$

$$\begin{pmatrix}\cos(\theta_0)\cos(\phi_0) & -\sin(\phi_0) & \sin(\theta_0)\cos(\phi_0)\\ \cos(\theta_0)\sin(\phi_0) & \cos(\phi_0) & \sin(\theta_0)\sin(\phi_0)\\ -\sin(\theta_0) & 0 & \cos(\theta_0)\end{pmatrix} \times$$

$$\begin{pmatrix}\sin(\chi)\cos(\psi)\\ \sin(\chi)\sin(\psi)\\ \cos(\chi)\end{pmatrix} \quad (14)$$

The atom is then tracked to the next step when the new energy and direction are calculated, and then the operation is repeated.

The recurrent computation is performed until the ejected particle slows down to energy equal to or less than the background gas's mean thermal energy (~ 0.038 eV). Then, further sputtering particle scattering is isotropic, and the atom's trajectory is determined until it deposits on the substrate. Likewise, 10^5 atoms' paths have been simulated. The entire arriving atoms on the substrate are determined at the end of the numerical simulation, and its variables (position, direction, energy, and the number of particles) are saved.

Finally, the recorded data is used to compute all of the characteristics of the atoms at the substrate level.

The present model assumes elastic collisions between sputtered atoms and background gas atoms, neglects interactions between sputtered particles, and ignores the thermal motion of the background gas. These assumptions are valid under low-to-moderate pressure conditions where the density of sputtered species remains significantly lower than that of the working gas. At higher pressures, inelastic collisions and particle–particle interactions may further enhance energy attenuation and angular isotropization, reinforcing the trends observed in this study.

3. Simulation Geometry and Process Parameters

Target and the substrate IZ were varied between 8, 12, 16 and 20 cm and the volume pressure were varied between 0.3, 0.5, 0.8 and 1 Pa. Metals targets (Cu, Al and Ag) and semiconductor targets (Ge, Te and Si) were sputtered by 262 eV pure Argon (Ar+) with normal incidence angle. Argon ions formed in the plasma bombard the targets and eject metals and semiconductors atoms that are then deposited on the substrate.

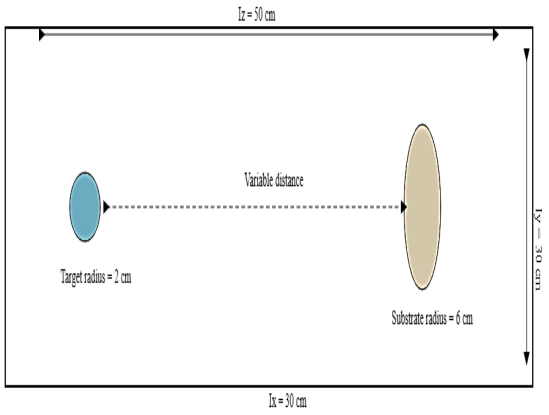

Fig. 1: Model used on the simulation

4. Results and Discussion

Each simulation was performed using 10^5 sputtered particles to ensure statistical convergence. Arrival energy distributions were normalized to the total number of particles reaching the substrate, and repeated test runs showed variations below 3% in arrival counts, indicating stable Monte Carlo convergence.

All energy distributions are normalized to the total number of atoms reaching the substrate to allow direct comparison between different pressures and target–substrate distances.

An atom exits the target with an energy and direction after which it undergoes collisions. The collisional transport is

stopped when the atom arrived at the substrate after which its properties (position, direction, energy and number of collisions) are stored in separate files.

The nascent energy and angular distribution of sputtered particles is taken from the analytical model of Sigmund–Thompson. This model calculates the ejection of particles from a solid due to a well-developed collision cascade. From this approach, it follows that the energy and angular parts of the distribution are separable, i.e. there is no angular dependence of the energy distribution.

4.1. Variation of target–substrate distance

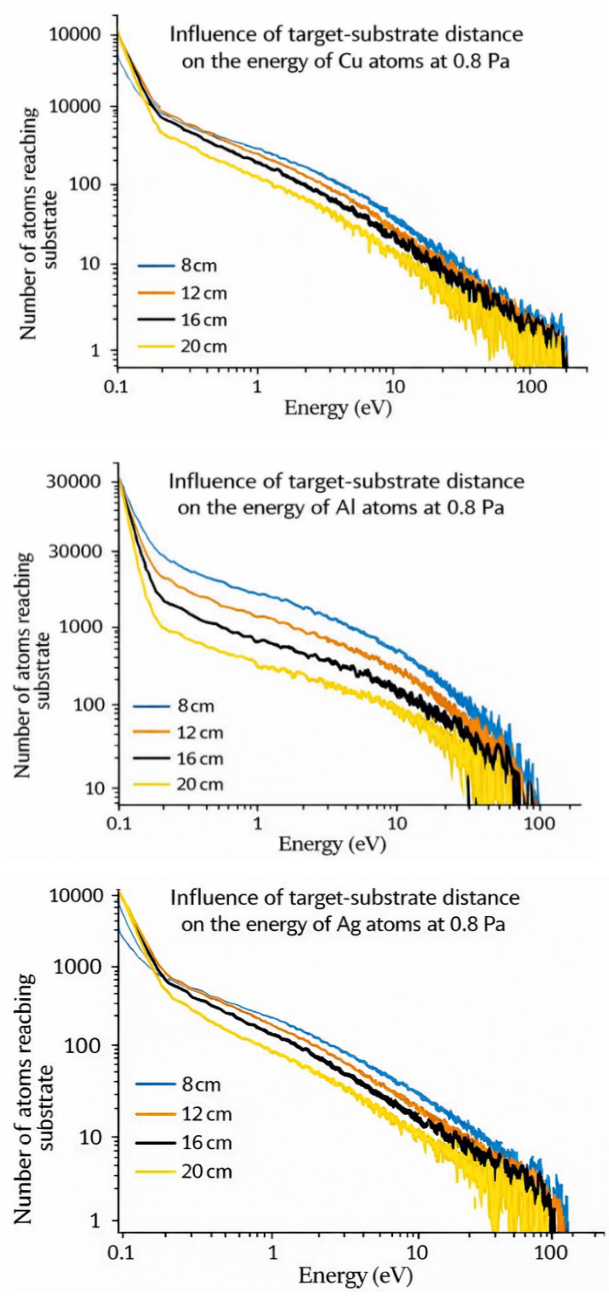

Fig. 2: The energy distribution as a function of target– substrate distance for arriving atoms of a: Cu, b: Al and c: Ag.

Figure 2 shows the simulation results of the sputtered metals atoms (Cu, Al and Ag) arriving at the substrate for different conditions of target–substrate distances IZ, and Figure 3 shows the simulation results of the sputtered semiconductors atoms (Ge, Si and Te).

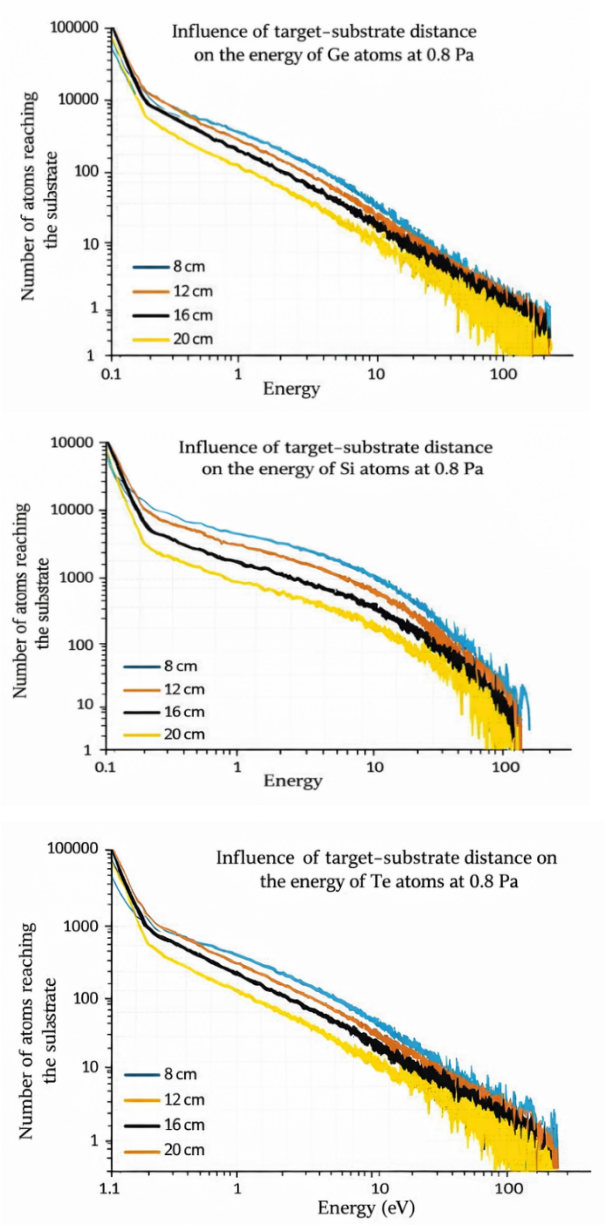

Fig. 3: The energy distribution as a function of target–substrate distance for arriving atoms of a: Ge, b: Si and c: Te.

When 0.8 Pa pressure is applied, the graphs shows that with an increase in the target–substrate distance (IZ), the number of sputtered atoms arriving at the substrate decreases (for example, the number of Al global sputtered atoms arriving at the substrate for a target–substrate distance of 8 cm was 156,220, however, for 20 cm it was 70,086) and same for Ag, Cu, Ge, Te and Si but with different magnitudes.

Also, we can observe that increasing the distance will

increase the number of collisions between the energetic ions and the thermal gas atoms (Ar atoms) through the vacuum of the deposition chamber which led to losing an important amount of their kinetic energy in the process and shifts the energy distribution to lower values.

While these collisions are random, so probably some ions may have less collisions than others, and arriving at the substrate with higher energies causes a significant variation of the energy distribution in the range from 10 eV to 100 eV for both metals and semiconductors atoms.

4.2. Variation of chamber pressure

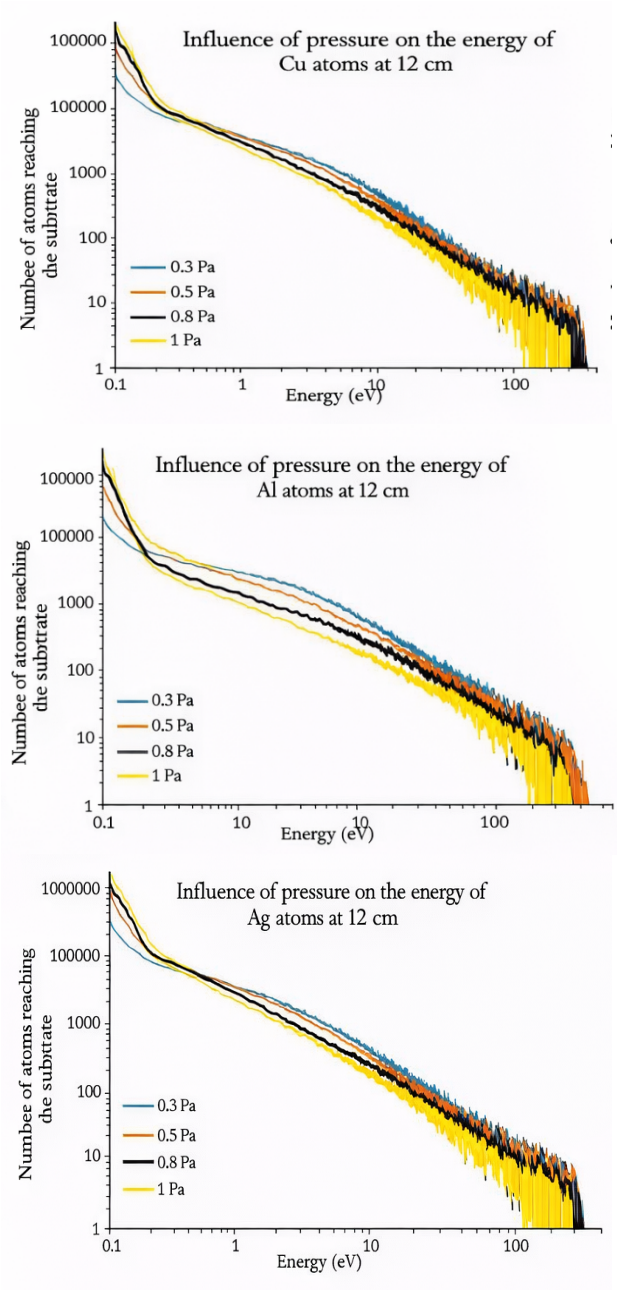

Fig. 4: The energy distribution as a function of pressure for arriving atoms of a: Cu, b: Al and c: Ag.

Figures 4 and 5 show, respectively, the simulation results of the sputtered metals atoms (Cu, Al and Ag) and sputtered semiconductors atoms (Ge, Si and Te) arriving at the substrate for different chamber vacuum pressures. The energy of the Ar+ ions, the target diameter and the substrate diameter are again fixed at 262 eV, 5 cm and 40 cm, respectively.

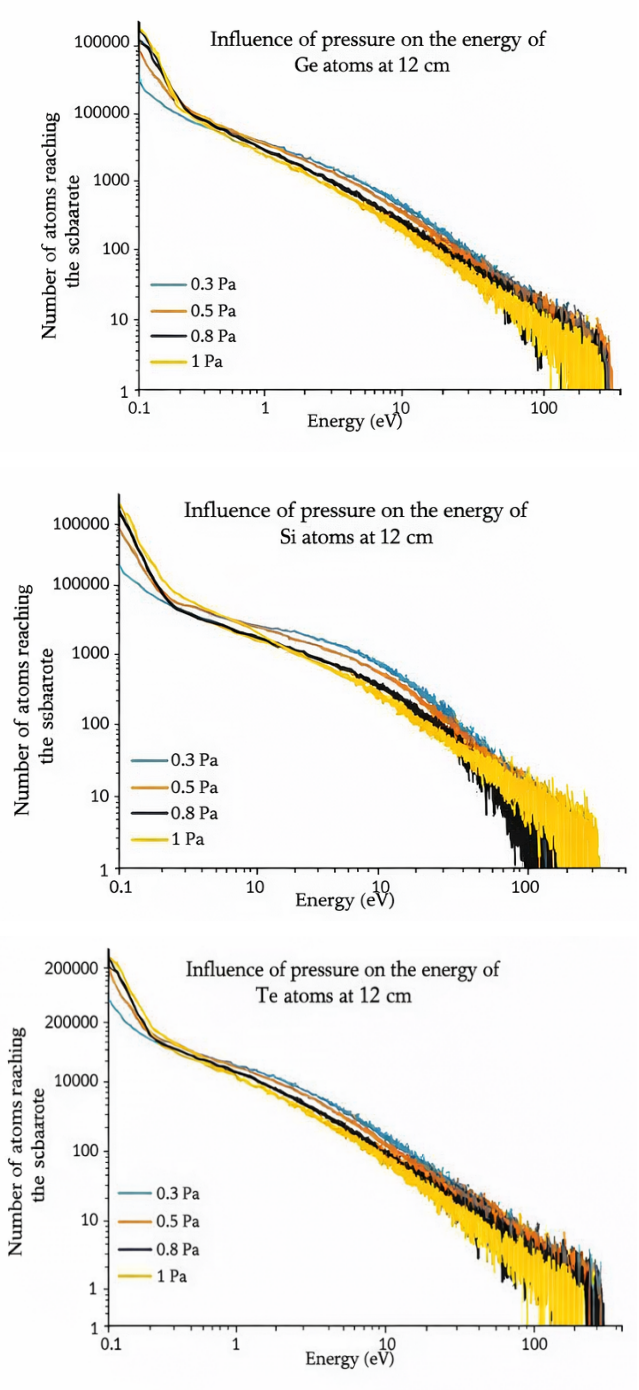

Fig. 5: The energy distribution as a function of pressure for arriving atoms of a: Ge, b: Si and c: Te.

Before it is deposited, the sputtered atom undergoes a number of collisions with the background gas atoms; this

number is an important parameter because every collision induces trajectory and energy variations. When 12 cm of target– substrate distance (IZ) is applied, the graphs show that with an increase in the sputtering pressure (0.3, 0.5, 0.8 and 1 Pa), the numbers of the sputtered metals and semiconductors atoms arriving at the substrate decrease (Al global sputtered atoms arriving at the substrate for 0.5 Pa of pressure were 150,039 in number, however for 1 Pa, they were 106,620) and this is similar for Ag, Cu, Ge, Te and Si but with different amounts. Also, we can observe that increasing the pressure led to an increased number of collisions and also gradually losing an important number of ions' kinetic energy in the transportation phase toward the substrate and also shifts the energy distribution to lower values for both metals and semiconductors atoms.

5. Conclusion

With the development of smaller technologies, semiconductor layer depositions are used in several demanding applications such as integrated circuits, transistors, diodes and RF appliances used in very high-speed devices, and metal layer de- positions are used in the manufacture of different kinds of transportation, jewellery and contacts and also in construction, household items and consumer electronics. The microstructures of these films have been the intention of our group in order to help industrial practitioners by accounting for key parameters such as target–substrate distance and chamber pressure, which significantly influence film morphology and deposition uniformity.

The simulation with a Monte Carlo code has been applied in order to calculate the energy and the number of sputtered particles arriving at the substrate, which are both important parameters influencing the microstructure of the deposited thin film layers.

A circular target with 5 cm in diameter and substrate with 40 cm in diameter were installed in a cuboid vacuum chamber.

The simulated data results were validated by comparing them with the results by other authors like Mahieu et al.,1 who applied a Monte Carlo code to simulate the transport of atoms in DC magnetron sputtering to study the thickness profiles, on one hand, and to simulate the energy and direction of sputtered particles arriving at the substrate, on the other hand.

It was shown that for pressures between 0.3 Pa and 1 Pa and target–substrate distances of 8–20 cm, corresponds well with the results found by the above group. Moreover, this work has also shown that the pressure and the distance between target and substrate are the two very important factors to indirectly influence film growth mechanisms through changes in particle energy and angular distributions, according to established thin-film growth models of the deposited metal or semiconductor layers highly used in this ever-changing world and development processes.

In reality, in addition to these two factors influencing the sputtering process, in future works we will also study the influences of other factors like temperature, other materials like dielectric layers used only in telecommunication development and the other sputtered gases like xenon, oxygen and nitrogen ions.

Future work will focus on extending the present model to include temperature effects, additional sputtering gases, and direct experimental validation through film thickness measurements, surface roughness analysis, and crystallographic characterization.

References

[1] M. Koulali, A. Bouazza, An In-Depth Analysis of Investigating and Simulating Thin Film Materials Using the Sputtering Process in Plasma Environments, International *Journal of Thin Film Science and Technology*, **14(2)**, 119-124 (2025). https://doi.org/10.18576/ijtfst/140207.

[2] A. Bouazza, Computational Modeling of Magnetron Sputtering for Thin-Film Materials: Optimizing Deposition and Analyzing Morphology, *Bull. Lebedev Phys. Inst.*, **51 (9)**, 324-333 (2024). https://10.3103/S1068335624600694.

[3] A. Bouazza, Characterizing the Relationship Between Sputtered Atom Flux Generated by Electrical Discharge in Plasma and Thin Film Deposition Quality, *International Journal of Thin Film Science and Technology*, **13(2)**, 95-100 (2024). https://doi.org/10.18576/ijtfst/130202.

[4] A. Bouazza, Optimization of the Cathodic Sputtering Process for Fabricating Thin Film Materials used in Modern Photovoltaic Applications, *International Journal of Thin Film Science and Technology*, **13(2)**, 101-105 (2024). https://doi.org/10.18576/ijtfst/130203.

[5] A. Bouazza, Enhancing the Sputtering Process with Plasma-Assisted Electrical Discharge for Thin Film Fabrication in Advanced Applications, *International Journal of Thin Film Science and Technology*, **13(1)**, 13-16 (2024). https://doi.org/10.18576/ijtfst/130102.

[6] A. BouazzaAn Investigation by Monte Carlo Simulation of the Sputtering Process in Plasma. *J. Surf. Investig.*, **17 (5)**, 1172–1179 (2023). https://doi.org/10.1134/S1027451023050361.

[7] A. Bouazza, 3D Visualization of the Effect of Plasma Temperature on Thin-Film Morphology, *Bull. Lebedev Phys. Inst.*, **50 (1)**, 7-13 (2023). https://doi.org/10.3103/S1068335623010037

[8] A. Bouazza, Investigation using Monte-Carlo codes simulations for the impact of temperatures and high pressures on thin films quality, *Rev. Mex. Fís.*, **69 (2)**, 021501 1-12 (2023).

https://doi.org/10.31349/RevMexFis.69.021501

[9] A. Bouazza, Simulation of the Deposition of Thin-Film Materials Used in the Manufacturing of Devices with Miniaturized Circuits. *J. Surf. Investig.*, **16 (6)**, 1221–1230 (2022). https://doi.org/10.1134/S1027451022060283

[10] A. Bouazza, Deposition of Thin Films Materials used in Modern Photovoltaic Cells, *International Journal of Thin Film Science and Technology*, **11(3)**, 313-320 (2022). https://doi.org/10.18576/ijtfst/110308

[11] A. Bouazza, Sputtering of semiconductors, conductors, and dielectrics for the realization of electronics components thin-films, *International Journal of Thin Film Science and Technology*, **11(2)**, 225-232 (2022). https://doi.org/10.18576/ijtfst/110210

[12] S. E. C. Refas, A. Bouazza, and Y. Belhadji, 3D sputtering simulations of the CZTS, Si and CIGS thin films using Monte-Carlo method, *Monte Carlo Methods Appl.*, **27 (4)**, 373–382 (2021). https://doi.org/10.1515/mcma-2021-2094

[13] A. Bouazza and A. Settaouti, Understanding the contribution of energy and angular distribution in the morphology of thin films using Monte Carlo simulation, *Monte Carlo Methods Appl*, **24 (3)**, 215-224 (2018). https://doi.org/10.1515/mcma-2018-0019

[14] A. Bouazza and A. Settaouti, Monte Carlo simulation of the influence of pressure and target-substrate distance on the sputtering process for metal and semiconductor layers, *Mod. Phys. Lett. B*, **30 (20)**, 1–18 (2016). https://doi.org/10.1142/S0217984916502535

[15] A. Bouazza and A. Settaouti, Study and simulation of the sputtering process of material layers in plasma, *Monte Carlo Methods Appl.*, **22 (2)**, 149–159 (2016). https://doi.org/10.1515/mcma-2016-0106

[16] C. Oh et al., Influence of oxygen partial pressure in In-Sn-Ga-O thin-film transistors at a low temperature, *J. Alloys Compd.*, **805**, 211–217 (2019). https://doi.org/10.1016/j.jallcom.2019.07.091

[17] Wang, Jing, et al., Modification of SRIM-calculated dose and injected ion profiles due to sputtering, injected ion buildup and void swelling, *Nuclear Instruments and Methods in Physics Research Section B: Beam Interactions with Materials and Atoms*, **387**, 20-28 (2016). https://doi.org/10.1016/j.nimb.2016.09.015

[18] J. O. Achenbach et al., Correlative experimental and theoretical investigation of the angle-resolved composition evolution of thin films sputtered from a compound Mo2BC target, *Coatings*, **9 (3)**, 206 **(**2019). https://doi.org/10.3390/COATINGS9030206

[19] G. Hobler et al., Probing the limitations of Sigmund's model of spatially resolved sputtering using Monte Carlo simulations, *Phys. Rev. B.*, **93 (20)**, 1–17 (2016). https://doi.org/10.1103/PhysRevB.93.205443

[20] P. Meakin and J. Krug, Three-dimensional ballistic deposition at oblique incidence, *Phys. Rev. A.*, **46 (6)**, 3390–3399 (1992). https://doi.org/10.1103/PhysRevA.46.3390

[21] N. Nedfors et al., The influence of pressure and magnetic field on the deposition of epitaxial TiBx thin films from DC magnetron sputtering, *Vacuum*, **177**, 109355 (2020). https://doi.org/10.1016/j.vacuum.2020.109355

[22] J. F. Ziegler et al., SRIM - The stopping and range of ions in matter, *Nucl. Instruments Methods Phys. Res. Sect. B Beam Interact. with Mater. Atoms.*, **268 (11–12)**, 1818–1823 (2010). https://doi.org/10.1016/j.nimb.2010.02.091

[23] A. Siad, A. Besnard, C. Nouveau, and P. Jacquet, Critical angles in DC magnetron glad thin films, *Vacuum*, **131**, 305–311 (2016). https://doi.org/10.1016/j.vacuum.2016.07.012